Author’s accepted manuscript

Hydraulic and Hydromechanical Laboratory Testing of Large Crystalline Rock Cores

Johan Thörn, *Division of GeoEngineering, Chalmers University of Technology*
SE-412 96 Gothenburg, Sweden. johan.thorn@chalmers.se. Tel: +46 31 772 2040
Lars O Ericsson, Professor, *Division of GeoEngineering, Chalmers University of Technology*
Åsa Fransson, Professor*, Division of GeoEngineering, Chalmers University of Technology*

Abstract

In this paper, fracture stiffness in rock samples is determined by means of hydromechanical (HM) laboratory testing. The aim is threefold: to develop a procedure for sampling, to update testing equipment and to relate fracture stiffness to the geological history (e.g. stress history and fracture infillings). The hydraulic properties of twenty rock cores (diameter 190 mm, c. 100 mm high) from the Äspö Hard Rock Laboratory (HRL) were tested in a permeameter cell under different isotropic pressures up to 2.5 MPa. The flow rate through individual fracture samples was recorded. Four of the samples were re-tested in the permeameter cell using an updated hydromechanical procedure with deformation measurement across the fracture. Four load cycles of gradually increasing cell pressure were applied, resulting in a clearly observed hysteresis effect in the first and second cycles. Hydraulic aperture changes calculated using the cubic law were compared with their mechanical equivalents. The aperture changes followed similar trends, although these differed between the samples. Fracture stiffness was determined from the tests and the stiffness to hydraulic aperture relationship was found to follow previously published patterns linked to the storativity of fractures. Differences in stiffness are explained in the context of the geological history of individual samples, particularly their stress history. The paper presents a conceptualisation of the stiffness behaviour, which includes flow properties, geometric properties and the geological stress history of the tested samples.

Keywords:

Hydromechanical coupling, Fracture stiffness, Hydraulic aperture, Fracture deformation, Laboratory testing

1 Introduction

The hydromechanical (HM) behaviour of rock fractures has been the subject of numerous laboratory experiments over the last few decades, e.g. (Pyrak-Nolte et al. 1987; Iwano and Einstein 1995; Lamas 1995; Iwai 1976; Makurat et al. 1990; Raven and Gale 1985; Li et al. 2008). Heiland (2003) provides a review of hydromechanical laboratory experiments, including coupling between stress-dependent permeability changes in rock samples on a laboratory scale. A review of work carried out on fractured rock applications of hydromechanical coupling, focusing on the *in situ* scale, can be found in Rutqvist and Stephansson (2003). Zimmerman and Main (2003) present the general theoretical background to the hydromechanical behaviour of fractured rock. Zang and Stephansson (2010) provide a background to rock stresses.

The mechanical and hydrological behaviour of a rock fracture is determined using several parameters related to the geometry of the void space between the adjacent surfaces of a fracture. Hakami (1995) mentions eight such parameters: aperture, which is the distance between the surfaces; the contact area between the surfaces; the roughness and matedness of the surfaces, i.e. how coarse the surfaces are and how well they fit together; the spatial correlation length of the aperture; the presence of channelling, i.e. wider, continuous paths that may transmit water; the tortuosity of the flow paths and the fracture stiffness, which is a measure of the stress needed to bring the fracture surfaces one unit of length closer to each other. Fracture-filling minerals that may be precipitated in fractures is another factor that affects mechanical and hydrological behaviour. The geometric properties and the fillings, all dependent on the geological history of the fracture, are intricately connected and need to be accounted for when describing the mechanical and hydrological properties of rock fractures.

The water-conducting ability of a rock fracture can be expressed as the hydraulic aperture. The cubic law (e.g. Snow 1968) is a common idealisation of the hydraulic aperture as the solution to the Navier-Stokes equations for a constant distance between two smooth parallel plates between which laminar flow occurs. Even though traditionally the cubic law concept has been regarded as being valid from a hydraulic point of view (Witherspoon et al. 1980), it has no direct link to mechanical behaviour as mechanical loads cannot be transferred between two smooth, levitating surfaces.

Since hydraulic and mechanical properties can be expected to change at low effective rock stresses, it is important to include both sets of properties in an engineering description of a fracture system that is potentially water-bearing (e.g. for grouting). As Zimmerman and Main (2003) point out, the link between mechanical and hydraulic properties is indirect and there does not seem to be any simple general correlation between mechanical and hydraulic properties. Efforts have been made to establish a link between the hydraulic and mechanical apertures of rock fractures. An example of this is provided by Barton et al. (1985), updated in Olsson and Barton (2001), showing an empirical link using the joint roughness coefficient, JRC. Another example are cubic law-based models, see e.g. Konzuk and Kueper (2004), for the evaluation of certain models. Pyrak-Nolte and Morris (2000) set fracture flow properties in relation to fracture stiffness in the light of aperture correlation.

The aim behind the experiments described in this paper is to develop and improve a sampling and testing method that provides information on hydraulic aperture variation linked to mechanical aperture variation in a fracture normal stress range of 0-2.5 MPa. This study relates to the behaviour of fractures in granitic rock and includes fractures subject to low-stress compression and in a state of normal consolidation. It is proposed that unmated fractures, where the surfaces fit each other poorly, have large apertures and low normal stiffness. Well-mated fractures, where the surfaces fit each other well, are assumed to have a small aperture and large normal stiffness.

The materials and methods section of the paper describes certain geological data, e.g. on fracture sets. The samples are described as well as the experimental set-up, experimental workflow and data collection. The materials and methods section concludes with a description of the concepts and equations used for data analysis and conceptualisation, i.e. transmissivity, storativity, cubic law hydraulic aperture, fracture stiffness and fracture aperture distributions. The results section contains an account of the validity of various aspects of the experimental set-up as well as results from the hydraulic and hydromechanical experiments in terms of hydraulic apertures, mechanical deformations and calculated fracture stiffness values.

2 Materials and methods

Äspö Hard Rock Laboratory (Äspö HRL), situated on the island of Äspö in south-eastern Sweden (Figure 1), is a research facility operated by the Swedish Nuclear Fuel and Waste Management Co., SKB. The experiments presented here were performed on 19 rock core samples from the TASS Tunnel[1] and one from the TASQ Tunnel, both at Äspö HRL, at a depth of approximately 450 m. All core samples had a diameter of 190 mm and a height of about 100 mm, which gave an average area of the tested fractures of around 190 cm^2.

2.1 Site

The TASS Tunnel at Äspö HRL was excavated to demonstrate a procedure for sealing fine fractures (Funehag and Emmelin 2011). Consequently, a site was selected that provided good rock, low amounts of water and a favourable stress situation. The tunnel was excavated using the drill and blast method. The blasting itself was a demonstration of careful blasting, closely following the horseshoe contour and with minimal damage to the contour (Karlzén and Johansson 2010). The main rock type in the tunnel is a quartz monzodiorite, called Äspö diorite (Hardenby and Sigurdsson 2010).

The fractures in the Äspö area rock mass, which was formed about 1.8 Ga ago, were generated and filled with mineral precipitates during different periods. Drake and Tullborg (2009) outline six generations of fracture minerals. These mineral generations were formed during different phases of tectonic stress and temperature throughout history in both new fracture sets and in older, reactivated sets. Calcite is the dominating mineral for the latest fracture mineralisations and appears mainly in older, reactivated fractures. A WNW-striking set is common for fractures bearing calcite and other minerals as well as fractures with calcite only and it is therefore probably the youngest set (Munier 1995).

2.2 Samples

In the TASS Tunnel wall, eight blocks, 1.5 m high, 1 m wide and about 0.7 m deep, were sawn using a diamond wire saw to allow the zone of expected disturbance or damage from the blasting to be studied in detail (Olsson et al. 2009). The blocks were then sawn into 75 slabs in order to categorise blast fractures from the charge holes used in the tunnel blasting as well as blast-induced and natural fractures surrounding the tunnel. To distinguish between different natural fractures, a mapping survey was

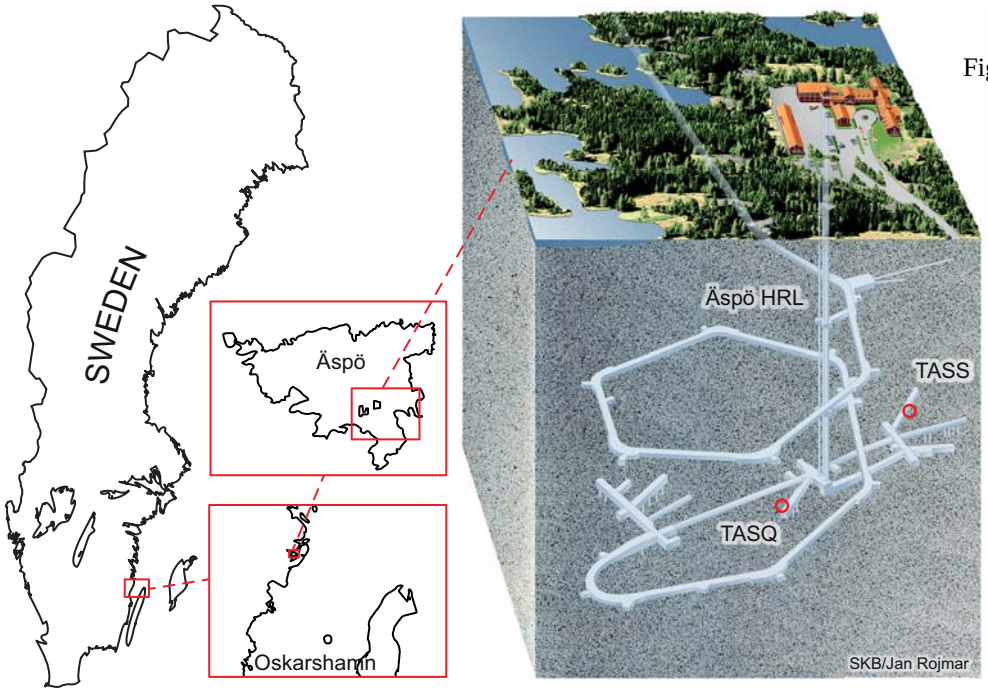

Figure 1: The location of Äspö in Sweden and the locations of the TASS and TASQ tunnels at Äspö HRL. Approximate sampling positions in TASS and TASQ are marked with red circles (The right-hand part of the figure is used with permission from SKB).

[1] The naming of the TASS Tunnel samples followed the convention used by SKB: PS0037061 means P (point object) S (tunnel S) 0037 (37 m along the tunnel axis) 06 (6th slab) 1 (first sample in slab). The naming of the tunnels is done in the same way, e.g. TASS = T (tunnel object) AS (Äspö) S (tunnel S).

conducted where the natural fractures were sorted into healed, tight (Ericsson et al., 2009 use the term closed) and open fractures. The filling minerals were then mapped (Olsson et al. 2009; Ericsson et al. 2009).

Core samples with a diameter of 190 mm were drilled from the approximately 100 mm thick slabs. Prior to drilling, a steel plate was fastened across the fracture to reduce potential damage from drilling on the fracture surfaces. The sampling positions were chosen in such a way that one fracture would cut through the centre of each sample. Natural open, tight and healed fractures were sampled, as well as blast-induced fractures. The hydraulic conditions in 20 such fracture samples were tested in a permeameter cell. Four of the samples were retested in hydromechanical experiments, where the permeameter was equipped with a mechanical deformation sensor. Samples with an array of different apertures, both mated and unmated, were used during the hydromechanical testing in order to cover a fairly wide aperture range.

The samples for hydromechanical testing were selected based on the results of the initial permeameter testing published in Ericsson et al. (2009). The sample selection favoured cores cut into two half-cylinders by one fracture. Three samples from the TASS Tunnel and one from the TASQ Tunnel were chosen for the coupled hydromechanical permeameter testing. The sampled fractures from the TASS Tunnel belong to a sub-horizontal fracture set dominated by open, water-bearing fractures (Rhén et al. 1997) containing calcite, chlorite and prehnite, suggesting that they may have been formed or reactivated during the past 450 Ma (Drake and Tullborg 2009).

2.3 Equipment

There are different ways of carrying out hydromechanical laboratory tests on rock samples. The review by Heiland (2003) distinguishes three general types of experimental set-ups: 1) hydrostatic compression, where a sample is subjected to the same stress in all three dimensions; 2) triaxial compression, where the axial and circumferential stress levels can be set individually; 3) uniaxial strain, where the lateral strain of the sample is kept constant by adjusting the confining pressure. The experiments conducted in this study fall into the first category, i.e. hydrostatic compression.

The permeameter consisted of a stainless steel cell (Figure 2, Figure 3), where isotropic pressure could be set up to 2.5 MPa. For safety reasons, the cell was filled with water and the cell pressure was applied to the water using a small volume of compressed air. The cell water was dyed, enabling detection of leakage into the sample. Water for the flow test was led into the sample from below and distributed across the bottom via a milled depression with a steel mesh. The same type of mesh was used in the lid to collect the water in a pipe that protruded from the cell. For the hydromechanical procedure, a deformation sensor was mounted in plastic brackets, which were epoxy-glued to the sample, perpendicular to the fracture trace in the centre of the top surface of the core. The sensor and brackets were housed in a milled hole in the lid. A Microstrain DVRT® with a stroke of 3 mm and resolution of 1.5 µm was used for deformation (Δa) measurements across the fractures. Calibration was performed using 0.1 and 0.15 mm thickness gauges after the sensor was mounted but before the top plate was put in place. See schematic representation of the experimental set-up in Figure 2 and the cutaway photo montage of the cell in Figure 3.

The internal fluid pressure loss across the sample is denoted *dh,* and was measured using a sensor placed at the same height as the outflow from the cell. In the experimental set-up, *dh* was defined as the height difference between the water table in the supply container and the outflow from the cell. The value of *dh* was kept constant mainly by raising the container at the same rate that the water level in the container decreased. A secondary solution, used for the samples with small apertures, was to apply compressed air in the supply container, see Figure 2.

To mount the core in the cell, it was placed on the steel base. The displacement sensor was fitted into the brackets and the steel lid was placed on the sample. Two latex rubber membranes were carefully applied by vacuum-sucking the membrane to the inside of a 210 mm pipe and then releasing the vacuum and the membrane around the sample. The ends of the membrane were folded, resulting in four layers of membrane. On the steel base and top plates of the cell, the membranes were tightened using rubber O-rings. The tightness of the set-up was tested using a solid plastic sample dummy under a confining pressure of 2 MPa and an internal pressure, *dh*, of 0.25 MPa. Over a period of one hour, 0.30 g of water collected at the top end of the cell. The water had found its way into the sample either from the cell or along the inside of the membranes. This corresponds to a transmissivity of less than $2*10^{-12}$ m^2/s. A potential leakage of that magnitude can be ignored for the hydromechanically

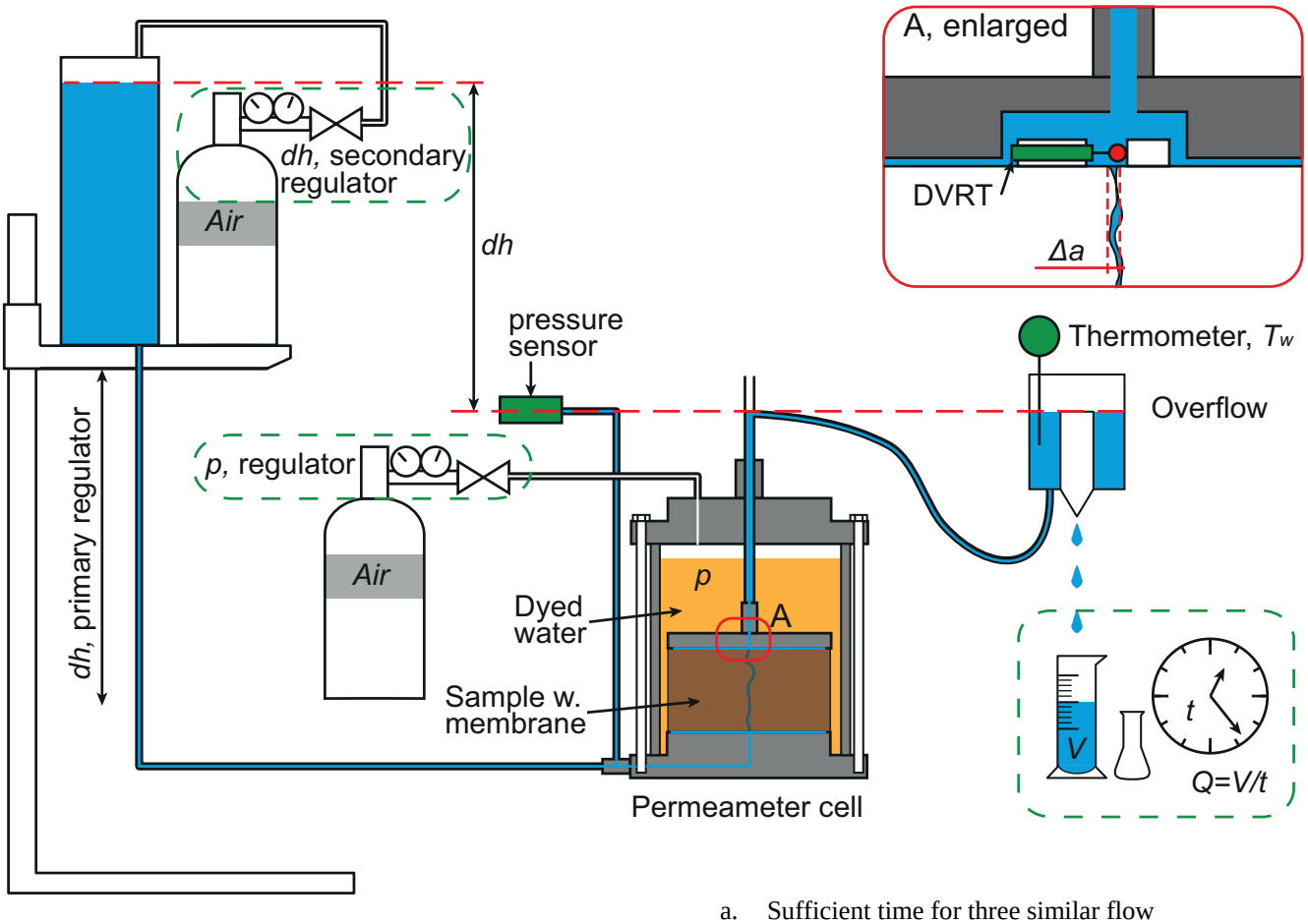

Figure 2: Sketch of the experimental set-up. The enlarged part, A, corresponds to the hydro-mechanical procedure, including mechanical deformation measurement. Compressed air was used to regulate *dh* when elevating the container was insufficient.

tested fractures since these had flow rates corresponding to $T > 10^{-9}$ m^2/s. The tightest samples in the initial hydraulic testing are close to this measurement limit and need to be used with caution.

2.4 Experimental procedure

A step-by-step working procedure for the HM experiments can be found in Thörn (2012). The initial hydraulic testing was conducted at a pressure in the cell of 0.5 and 1.0 MPa for most samples. The hold times for each pressure varied between the samples. Two of the initial tests and the subsequent hydromechanical testing had multiple pressure steps in four load cycles, see Figure 4. The time span was chosen as a trade-off between achieving stationary conditions and completing an entire test in one day. Test times were adjusted by varying the size of the container to be filled. The following two conditions were applied:

a. Sufficient time for three similar flow readings of a volume taking 1-5 minutes to fill: 100, 50, 20, 10 or 2 ml, depending on the aperture.
b. Sufficient time to achieve a stable reading on the deformation logger, about 10-30 minutes.

The *dh* pressure head was collected at a rate of one reading per second and plotted on a screen. The water storage container was lifted so that the water level in the container and the pressure head remained constant relative to the sample (see Figure 2). Deformation data were also collected at a rate of one reading per second and plotted on the screen. The flow volume was measured using graded measurement cylinders (100 ml, 50 ml and 20 ml) and Erlenmeyer flasks (10 ml and 2 ml). The time to fill was recorded using a time stamp macro in a Microsoft Excel spreadsheet, running on the same computer as the logging software for *dh* pressure and *Δa* deformation, which yielded a synchronised time value for all data sets.

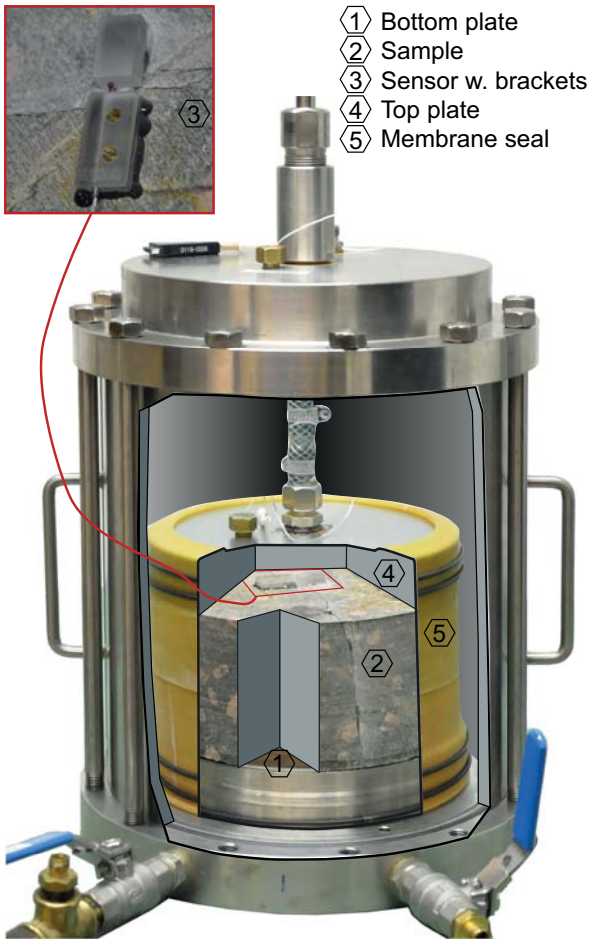

Figure 3: Cutaway photo montage of the cell with a sample.

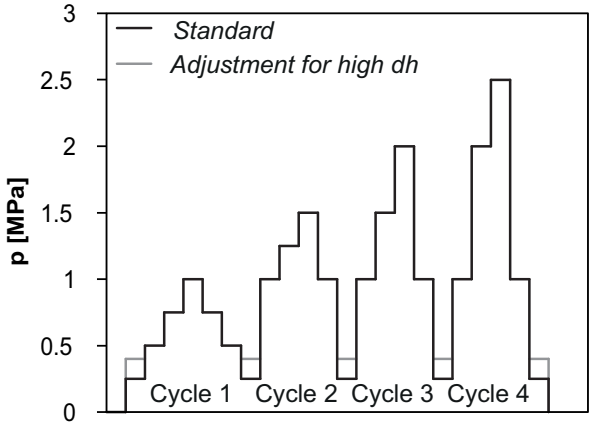

Figure 4: The pressure steps and cycles applied to the hydromechanical testing. The grey line represents an adjusted sequence used for samples with low transmissivity, where *dh* was set at 0.344 MPa, i.e. a 35.1 m head, while the other samples that followed the standard pressure cycles had a 0.65 m head.

2.5 Analysis methods

The output from the experiments was a flow rate measured as the volume of a container divided by the time taken to fill the container for each confining pressure. For the hydromechanical procedure, this was supplemented by a value for fracture closure, i.e. mechanical deformation. The confining pressure, *p*, and the sample pressure drop, *dh*, were predetermined and monitored throughout the testing, as was temperature.

The volume/time readings were asymptotically stabilising and consequently the final value in each step was used for further analysis. Transmissivity was calculated in accordance with Darcy's Law as the specific capacity *Q/dh,* taking into account fracture length, *L,* and width, *W*:

$$T = \frac{Q \cdot L}{dh \cdot W} \tag{1}$$

Rhén et al. (2008) used regression analysis to find an empirical link between storativity and transmissivity for borehole tests (Eq. 2). Using (Eq. 3) from Doe and Geier (1990), i.e. an expression that links storativity and fracture stiffness, Fransson (2009) established an expression of stiffness from transmissivity data. In (Eq. 3) the compressibility of water has been ignored. This was checked in Thörn (2012) and the difference in storativity from the compressibility of water is a maximum of 5% for PS0039023 and 1.5% for the other samples. A hydraulic test in a borehole section intersected by multiple fractures is expected to reflect one of the largest and least stiff fractures (Fransson 2009). The fractures sampled in this study were not necessarily the least stiff fractures in the vicinity of the sampling location.

$$S = 0.0109 \cdot T^{0.71} \tag{2}$$

$$k_n^S = \frac{\rho_w \cdot g}{S} \tag{3}$$

The Cubic-Law hydraulic aperture was calculated as:

$$b = \sqrt[3]{\frac{12 \cdot \mu_w \cdot T}{\rho_w \cdot g}} \quad (4)$$

where μ_w is the viscosity and ρ_w the density of water.

Hydraulic deformation for each pressure step can be calculated from the hydraulic aperture, *b*. The mechanical aperture, *a*, is unknown both in its initial state and under the various confining pressures. However, the change of aperture, *Δa,* relative to the beginning of the test is known. A hydraulic and mechanical fracture normal stiffness can be calculated for each pressure step as the aperture change per stress change (Pyrak-Nolte and Morris 2000, Zimmerman and Main 2003). This is adopted for both mechanical deformation, (Eq. 5) and change of hydraulic aperture, (Eq. 6).

$$k_n^a = \frac{\Delta p}{\Delta a} \quad (5)$$

$$k_n^b = \frac{\Delta p}{\Delta b} \quad (6)$$

3 Results

3.1 Validity and sensitivity of test conditions

Larsson (1997) derived the pressure across a fracture through a biaxially loaded cylindrical rock sample as a homogenous normal pressure equal to the cell pressure. This is also valid for three-dimensional hydrostatic loading since the volumetric stress across the fracture is equal to the cell pressure. The effect of the water pressure inside the fracture is insignificant for most samples since this pressure is about 0.65 m water column and is significantly lower than the cell pressure. However, caution should be observed for the lowest confining pressure steps of the samples tested at *dh* = 35 m. Iwano (1995) conducted triaxial testing of rock cores and concluded that it did not seem to make a difference if the stress was applied as normal stress or confining stress. Consequently, in this analysis the confining pressure step change was used as the numerator in (Eq. 5 and Eq. 6), i.e. normal stress change.

The chosen stress range for the experiments, 0-2.5 MPa, is founded on a basic distinct element analysis of the stresses in the area of the sawn-out slot (Ericsson et al. 2009) using Examine 2D (Rocscience 2010) and assuming an idealised tunnel contour. Input was real stress data from the area of the TASS Tunnel as well as the size and orientation of the tunnel. The three secondary stresses were estimated to be in the range 0-7 MPa in the rock volume of the slabs where the samples were taken. An estimation using the positions and orientations of the sampled fractures, with an idealised tunnel contour, also resulted in normal and shear stresses in the range 0-8 MPa. For the hydromechanically tested samples, the normal and shear stresses were as follows: PS0037053 and PS0037061 = 1-1.5 MPa; PS0039023 = 4-8 MPa; PS0039061 = 3-5 MPa.

The equations used for flow in fractures require laminar conditions. The experiment parameters were checked for turbulence according to the criteria presented by Zimmerman and Bodvarsson (1996), adapted graphically in Gustafson (2012). The transition from laminar to turbulent flow is at about Reynolds number 1 for a rough surface, while the transition in the case of smooth parallel plates is at about Reynolds number 1150. These two transition criteria are included in Figure 5, where the hydraulic gradient, *i*, is plotted against the hydraulic aperture, *b*. Each cross represents one set of test conditions used in the experiments. The flow was found to be in the laminar regime, see Figure 5.

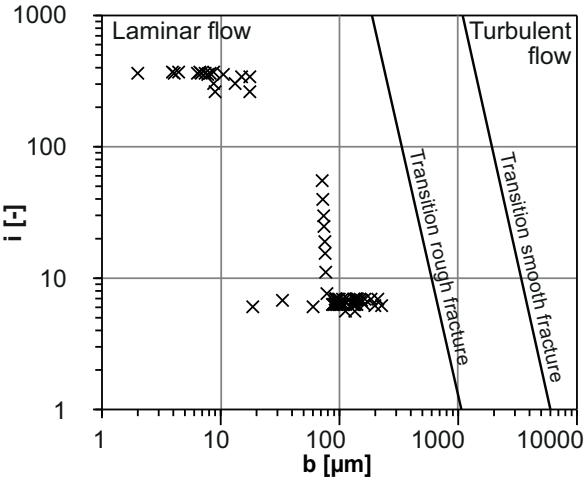

Figure 5: Graph showing the hydraulic aperture, and *dh*-pressure gradient, *i*, for the experiments. The flow through the samples can be regarded as laminar.

The flow value was measured three times at each pressure step. With few exceptions, flow readings two and three were lower than the first one or two readings for each confining pressure step. The third reading was used for further analysis, supported by the fact that the flow seemed to asymptotically approach a stable value.

A Monte Carlo simulation was performed on a dozen uncertainties related to the measured test conditions and values. Uncertainty was expressed in terms of a $\Delta b/\Delta a$ ratio. The largest contribution to the variance, i.e. to the simulated total uncertainty, was found to be assessing the representative time to fill the measurement cylinder, which is a consequence of the asymptotically stabilising flow. Expressed in terms of $\Delta b/\Delta a$ ratios of sample AB1AB2, the uncertainty for increasing-pressure steps was insignificant. For some of the decreasing-pressure steps the uncertainty was considerable and in general less reliable (Thörn 2012).

3.2 Hydraulic tests

The increase in confining pressure from 0.5 MPa to 1.0 MPa resulted in a reduced hydraulic aperture of the samples, corresponding to a closure of the fracture sample (Ericsson et al. 2009). For the two samples that were subject to cyclic loading during the hydraulic tests, PS0037061 and PS0039061, a hysteresis was experienced (Figure 6), and the behaviour resembled the behaviour described in the literature, see e.g. (Bandis et al. 1983).

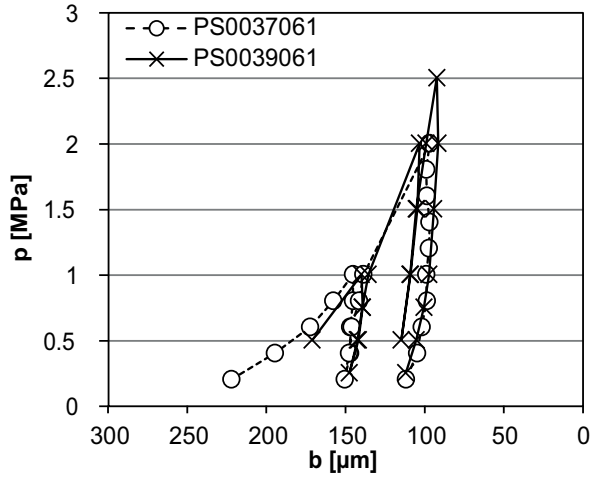

Figure 6: The cubic law hydraulic apertures for different cell pressures from cyclic permeameter testing. Two load cycles were run for sample PS0037061 and three load cycles for sample PS0039061.

3.3 Hydromechanical tests

In the experiments where both closure and hydraulic aperture were monitored, a gradually smaller at-rest hydraulic aperture for the load cycles was exhibited (Figure 7), similar to the initial tests. The simultaneously measured closure of the fractures showed the same behaviour for samples PS0037053 and AB1AB2 but with $\Delta b/\Delta a$ ratios of 0.65 and 1.9 respectively. For the small-aperture PS0039023, the closure was essentially elastic during the load cycles, with only a minor amount of permanent deformation and a fairly linear deformation path. The halves of this sample are joined, i.e. partially healed, which offers a reasonable explanation for the elastic appearance of the mechanical deformation and the small hydraulic deformation values. Numeric measurement values and pictures of the hydromechanically tested samples can be found in Thörn (2012).

3.4 Fracture stiffness

Fracture stiffness was calculated from the experiments using (Eq. 5) and (Eq. 6), (Figure 8, Figure 9), in the manner introduced by Fransson (2009). As an empirical reference, the hydraulic stiffness from storativity, (Eq. 2) and (Eq. 3), was included in the graphs. Eq. 2 relates transmissivity to storativity and is stated by Rhén et al. (2008) to be valid down to apertures of about 80 µm, since that was the smallest aperture in their data set. In this analysis it has been extrapolated beyond that. Broken lines corresponding to ± one order of magnitude of storativity (see Eq. 3) are also included in Figures 8-10. Since only *changes* in mechanical aperture were measured in the experiments, with no absolute value for the mechanical aperture, the stiffness based on mechanical deformation, k_n^a, is plotted on the *b*-axis in Figures 8-10.

Stiffness from changes in hydraulic aperture was calculated for the samples that were subject to only 0.5 and 1.0 MPa confining pressure, and the values are included in Figure 8. All data points in the figure are assigned a line that shows the apertures before and after the step. This is the aperture change used in the stiffness equations, (Eq. 5) and (Eq. 6).

A conceptual model of the stiffness behaviour for the samples subject to cyclic loading has been developed (see Figure 10). Furthermore, Table 1 presents comments on how the fracture geometry parameters (Hakami 1995) are dealt with in the model. A tentative 2D fracture trace was computer-generated based on Brownian motion and duplicated. The upper surface

trace was moved to mimic shear by displacement. Roughness (of one surface) and translation between two surfaces results in various degrees of matedness (see types (a)-(c) in Figure 10 and comments in Table 1). The resulting geometry gives rise to different correlation lengths, short for (a) and long for (c). Consequently, a large number of contact points are expected for (a) and a small number for (c). Type (a) resembles the comments Pyrak-Nolte and Morris (2000) made regarding fractures with no spatial correlation of aperture: the hydraulic aperture of this group is less dependent on stress or stiffness.

Aperture distribution and correlation length influence the (specific surface) area available flow area. In (a) the area is large, resulting in larger head losses and a smaller aperture. Similarly, a high level of tortuosity results in larger losses due to a longer flow path. This results in stiffness that is inversely proportional to the hydraulic aperture (Fransson 2009).

Figure 7: Results from hydromechanical testing of samples PS0037053, PS0039023, AB1AB2 and PS0039061. Four load cycles were run. Mechanical deformation, *Δa,* is on the upper horizontal axis, and hydraulic aperture, *b*, is on the lower horizontal axis. Note that the scales are different, with ratios of total hydraulic deformation/total mechanical deformation of approximately a) 0.65, b) 1.9, c) 0.15 and d)

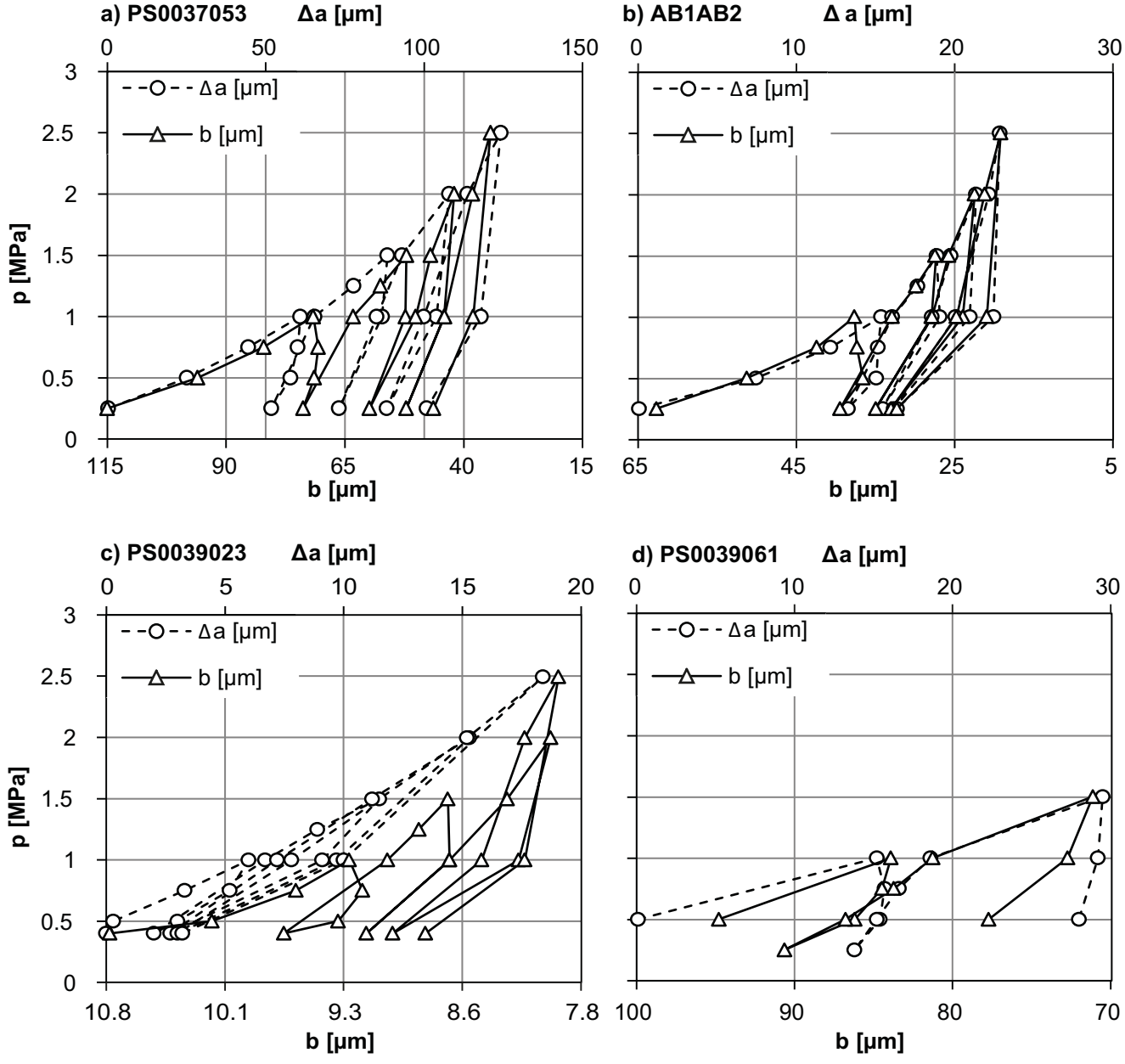

To replicate the situation where the three computer-generated fractures experienced the same low amount of normal load, the upper surface was lowered until 1% contact area was reached. For the three fractures, corresponding lognormal aperture distributions were generated, where the well-mated, (low-shear) fracture exhibited the most narrow aperture distribution. Distributions from Hakami (1995) and Hakami and Larsson (1996) were used to ensure that the generated aperture distributions were reasonable.

Interaction between the fracture geometry parameters (Hakami 1995) and how they are used in the context of Figure 10 is outlined in Table 1.

Table 1 Comments on fracture geometry parameters from Hakami (1995) for groups (a) and (c) in the conceptual model, and brief notes on how they are handled in the conceptual model, cf. Figure 10.

Sample PS0039023 revealed a small aperture and is compared to group (a) distribution in Figure 10. The mechanical stiffness was fairly constant, suggesting only minor effects on the contact geometry. The hydraulic stiffness on the other hand was increasing, suggesting that a residual aperture had been reached and that the increasing cell pressure resulted in smaller and smaller changes to the hydraulic aperture.

AB1AB2 and PS0037053 acquired stiffness in a similar way to the trend at Äspö and Laxemar, as described in Rhén et al. (2008) and Fransson (2009). It is assumed from this that the flow pattern changed significantly when the mechanical aperture decreased. This includes increased tortuosity. This type of behaviour is compared to the group (b) aperture distribution curve in Figure 10, where significant changes appear when new contact areas are created as a result of the deformation.

	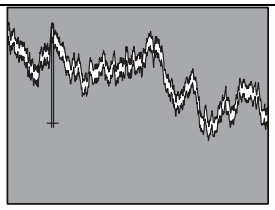	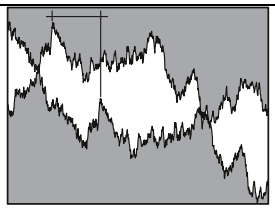	
Fracture geometry parameter	**Group (a) - Small translation, 1D flow**	**Group (c) - Large translation, 2D flow**	**Means of handling in model**
Matedness	Well-mated fractures	Unmated fractures, where shearing is assumed under low normal stress.	Definition of group (a)-(c) (main difference between groups)
Spatial correlation length of aperture	Shorter correlation length	Longer correlation length	Definition of group (a)-(c) (direct consequence of matedness)
Roughness	The model is inclined towards fractures in crystalline rock that has not been sheared under high normal stress and is currently under low normal stress. Comments are made on the possible behaviour of fractures that have lost some of the initial roughness, i.e. shearing or compression under high normal stress.		Delimitation
Contact area	All groups represent rough fractures with a small contact area.		Delimitation
Aperture	Small apertures	Hydraulic apertures are larger and can be described accurately using the cubic law.	Main parameter of model
Channelling, tortuosity	Close to a residual aperture, due mainly to stress-insensitive channels. Higher tortuosity	2D flow characteristics. Low tortuosity.	Definition of group (a)-(c)
Stiffness	High stiffness increase Ideal group (a) results are difficult to achieve on natural fractures since small dislocations can be expected due to sample extraction and handling.	Low due to a limited amount of contact area increase per closure.	Main parameter of the model

PS0039061 and PS0037061 showed a large aperture and a steep increase in stiffness while the large hydraulic aperture did not change to any great extent. This behaviour is explained as an increase in contact area from a growing number of contact points, keeping the tortuosity fairly constant and thus not affecting the hydraulic aperture significantly. This is in line with the conclusions drawn by Barton, where for large apertures or smooth surfaces the hydraulic and mechanical apertures are roughly equal (see e.g. Olsson and Barton 2001). The behaviour is compared to group (c) aperture distributions in Figure 10.

If the stiffness calculated from hydraulic data is cross-plotted to the stiffness from deformation data it is evident that the different samples follow different trends (Figure 11). The k_n^b/k_n^a ratios are around 20 for PS0039023, 2 for PS0037053 and 0.5 for AB1AB2 and PS0039061. AB1AB2 acquires more mechanical stiffness than hydraulic stiffness. In Figure 10, where AB1AB2 is described as acquiring contact points and tortuosity, the new contact area dominates. Sample PS0039023 is at the other end of the plot, acquiring more hydraulic stiffness than mechanical stiffness due to a small aperture close to a residual value that is unaffected in the stress range of the experiments.

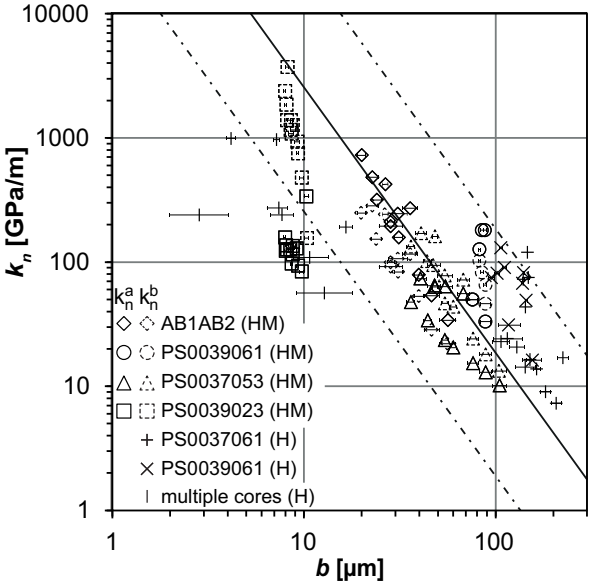

Figure 8 Stiffness data for samples that have undergone cyclical testing as well as the single-step samples (denoted 'multiple cores'). Each mark represents the stiffness for one pressure increase step. The line represents stiffness from storativity (Eq. 2) and (Eq. 3) and the broken lines one order of magnitude above and below. Stiffness is calculated as (Eq. 5) using hydraulic deformation data for all samples as well as mechanical deformation data for AB1AB2, PS0039061, second round, PS0037053 and PS0039023.

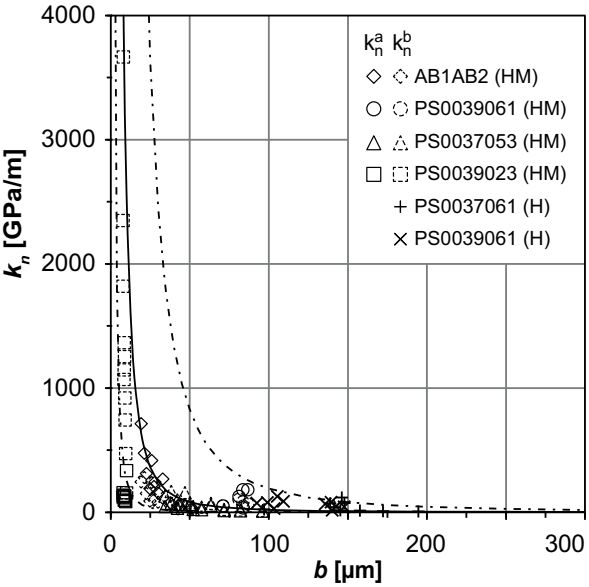

Figure 9: Same data as Figure 8 in a double linear plot, without the lines showing the calculation span. Here the large behavioural differences become evident, with high stiffness for low aperture fractures and low stiffness for high aperture fractures.

4 Discussion

A testing and sampling method was developed and applied. Both hydraulic and hydromechanical experiments were performed on fracture samples where information was available about the geology and orientation. The geological evolution of a fracture plays a significant role in the hydraulic and hydromechanical behaviour of the fracture and the hypothesis was that different behaviours would be exhibited by different fracture sets. Although each sample that was tested can be described in a geological context, the low number of samples cannot support any general conclusions with regard to geological history and set-specific properties. More tested samples that include all the prominent fracture sets and mineral fillings would enable a better link to be established with geological history. However, the general trend of low stiffness for large aperture fractures and high stiffness for low aperture fractures has been captured in the experiments.

The stiffness increases with increasing area of contact between the surfaces. This is achieved either by the contact points growing or the formation of new contact points, adding to the area in contact (See sample PS0039061, 'X' and 'O' in Figure 10). Growing points do not affect the aperture as significantly as if new contacts had been formed and which obstructed flow paths.

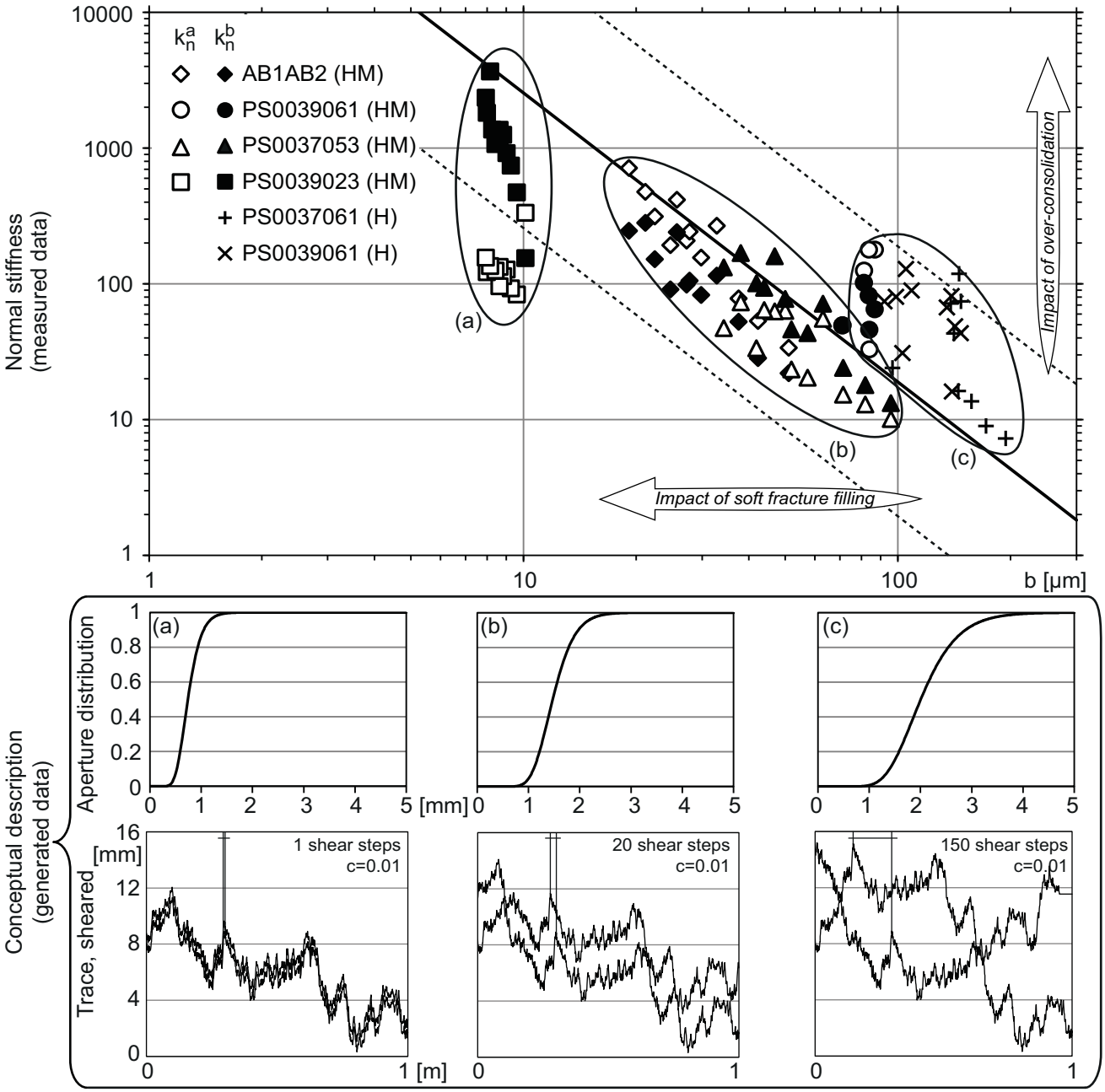

Figure 10: Top half: Same measurement data as Figure 8 and with a conceptual description of how the samples behave (bottom half). A tentative fracture trace is computer-generated, duplicated and displaced to mimic three amounts of shear. The upper generated surface is then lowered until 1% of the 'area' is in contact. The corresponding lognormal cumulative aperture distribution is shown. Group (a) corresponds to a large number of contact points and (c) to a small number of contact points that grow with increased load, producing increased stiffness but with no significant effect on tortuosity as no significant number of new points are generated. Group (b) corresponds to a case where new contact points arise, increasing the tortuosity and reducing the hydraulic aperture, while stiffness is acquired.

The experimental results mostly follow the fracture stiffness to hydraulic aperture relationship suggested by Fransson (2009) and were within ± 1 order of magnitude. The relationship is expected to be valid for fractures under low effective compressive stress and low levels of permanent deformation. The sample that deviated most from the relationship was PS0039023, which has the lowest aperture among the samples and is partially healed. The fact that PS0039023 was partially healed during the testing implies that it was not reactivated by the tunnel excavation. The open part of the fracture would therefore be over-consolidated from the pre-excavation stresses in the stress range of the experiments since the fracture has been hindered from substantial shear motion.

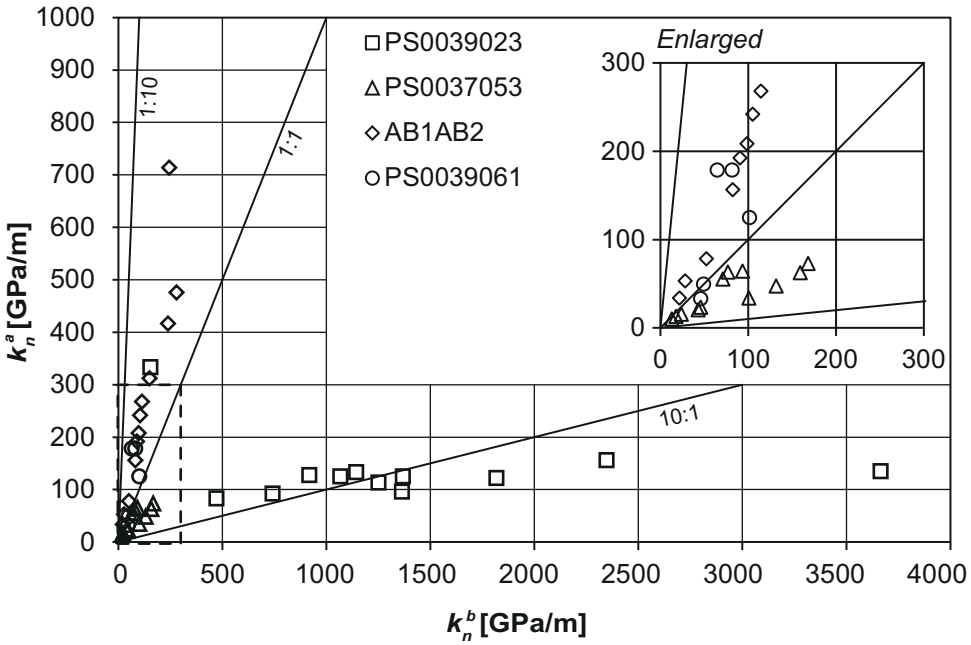

Figure 12: Cross-plot of hydraulic and mechanical apertures. Each sample seems to follow a certain trend.

Results from released pressure steps did not reflect behaviour that was as systematic as for the increasing pressure steps. At some steps none or very little rebound from the previous closure was exhibited, while other steps showed rebounds similar to the closure of the previous step. Given the experimental context of low stresses and few contact points, an explanation for sometimes having full rebound and sometimes practically no rebound is that there is a random element in the type of deformation. For some steps the deformation is entirely elastic with no permanent damage while for other steps a few mineral grains at the contact points are crushed, producing permanent deformation that does not rebound when the pressure is released. This is in line with the behaviour shown in other studies (e.g. Bandis et al. 1983), where permanent and resilient deformation is seen in the cycles. However, a thorough analysis of the mechanics behind each released-pressure step was beyond the scope of this study.

The experimental set-up used one deformation transducer placed near the point of half of the fracture width and the full height. It was thus assumed that no rotation of the sample halves occurred. To develop the equipment further, adding one or two more transducers to the bottom surface should be considered.

Moving from a real fracture *in situ* to a laboratory-scale sample is not inconsequential. Samples PS0037053 and PS0037061 for example are taken from the same fracture, in adjacent slabs, but they behave differently in the experiments. One explanation for this could be that the contact points supporting the fracture *in situ* are not sufficiently close to support the 100 by 190 mm samples. Small, handling-related dislocations could be another explanation.

A well-mated fracture is likely to have a large number of small contact points while an unmated fracture should have fewer contact points. If the shearing that unmates a fracture occurs under a sufficient amount of normal stress, some points in the fracture topography are sheared off. It is therefore likely that an unmated fracture has few larger areas of contact, while the mated one has a larger number of smaller areas. An extended analysis of the fracture surface geometries would be useful in order to couple to different geological signatures (i.e. orientation, stress history and infillings) of individual fractures and their hydromechanical behaviour. This includes topography measurements, providing statistical aperture distributions, as well as looking for kinematics. More samples from different fracture sets would also be beneficial. The work conducted in this paper could possibly develop towards assessing mechanical properties using hydraulic tests, which would be beneficial in tunnel construction.

5 Conclusions

Hydraulic aperture variation was coupled to mechanical aperture variation through stiffness for the normal stress range 0-2.5 MPa. The experimental study involved granitic fracture samples and the following conclusions are drawn from the results:

- The results support the hypothesis that a large-aperture fracture has low fracture normal stiffness, while a smaller aperture corresponds to high fracture normal stiffness. This is expected to be particularly true for fractures that have undergone translation and compression under low stress.
- Fracture stiffness calculated from the tests and stiffness in relation to hydraulic aperture were found to follow the trends linked to the storativity of fractures reported in Fransson (2009).
- The geological history, including stress history, fracture orientations, shearing and mineral precipitates affect the hydromechanical behaviour of different samples, which can be seen in the stiffness/aperture and normal stress/hydraulic aperture/mechanical aperture graphs.
- The previously known hysteretic behaviour of cyclic hydromechanical testing is captured in the experiments.
- The sampling method and experimental set-up that were developed were found to be robust.
- Errors were estimated to be small in the loading part of the cyclical testing while the unloading was found to be more sensitive.
- More work is needed on measuring surface topography and the number of samples would need to be expanded in order to make stronger claims.

6 Acknowledgements

The first author would like to acknowledge the following contributions: Petra Brinkhoff, for running the hydraulics-only experiments. Aaro Pirhonen and Peter Hedborg for building and helping to set up the equipment. Christine Räisänen, Robin Harder and Patrick O'Malley for feedback on the manuscript. Sara Kvartsberg for her help with coupling the fracture mapping. The Swedish Nuclear Fuel and Waste Management Co (SKB) for financial support, for providing the test site and samples and for feedback on the work.

7 References

Bandis SC, Lumsden AC, Barton NR (1983) Fundamentals of rock joint deformation. Int J Rock Mech Min Sci Geomech Abstr 20 (6):249-268. doi:10.1016/0148-9062(83)90595-8

Barton N, Bandis S, Bakhtar K (1985) Strength, deformation and conductivity coupling of rock joints. Int J Rock Mech Min Sci Geomech Abstr 22 (3):121-140. doi:10.1016/0148-9062(85)93227-9

Doe TW, Geier JE (1990) Interpretations of Fracture System Geometry Using Well Test Data, Stripa Project SKB TR 91-03. Swedish Nuclear Fuel and Waste Management Co, Stockholm, Sweden

Drake H, Tullborg E-L (2009) Fracture mineralogy Laxemar: Site descriptive modelling, SDM-Site Laxemar SKB R-08-99. Swedish Nuclear Fuel and Waste Management Co, Stockholm, Sweden

Ericsson LO, Brinkhoff P, Gustafson G, Kvartsberg S (2009) Hydraulic Features of the Excavation Disturbed Zone - Laboratory investigations of samples taken from the Q- and S-tunnels at Äspö HRL. SKB R-09-45. Swedish Nuclear Fuel and Waste Management Co, Stockholm, Sweden

Fransson Å (2009) Literature survey: Relations between stress change, deformation and transmissivity for fractures and deformation zones based on in situ investigations. SKB R-09-13. Swedish Nuclear Fuel and Waste Management Co, Stockholm, Sweden

Funehag J, Emmelin A (2011) Injekteringen av TASS-tunneln: Design, genomförande och resultat från förinjekteringen SKB R-10-39. Swedish Nuclear Fuel and Waste Management Co, Stockholm, Sweden

Gustafson G (2012) Hydrogeology for Rock Engineers. BeFo, Stockholm, Sweden

Hakami E (1995) Aperture distribution of rock fractures. Ph.D. Thesis, Royal Institute of Technology, Stockholm, Sweden

Hakami E, Larsson E (1996) Aperture measurements and flow experiments on a single natural fracture. Int J Rock Mech Min Sci Geomech Abstr 33 (4):395-404. doi:10.1016/0148-9062(95)00070-4

Hardenby C, Sigurdsson O (2010) Äspö Hard Rock Laboratory: The TASS Tunnel: Geological mapping. SKB R-10-35. Swedish Nuclear Fuel and Waste Management Co, Stockholm, Sweden

Heiland J (2003) Laboratory testing of coupled hydro-mechanical processes during rock deformation. Hydrogeol J 11 (1):122-141. doi:10.1007/s10040-002-0236-2

Iwai K (1976) Fundamental Studies of Fluid Flow Through a Single Fracture. Ph.D. Thesis, University of California, Berkeley CA

Iwano M (1995) Hydromechanical Characteristics of a Single Rock Joint. Ph.D. Thesis, Massachusetts Institute of Technology, Cambridge MA

Iwano M, Einstein H (1995) Laboratory Experiments on Geometric and Hydromechanical Characteristics of Three Different Fractures in Granodiorite. Paper presented at the 8th ISRM Congress, September 25 - 29, 1995, Tokyo, Japan

Karlzén R, Johansson E (2010) Slutrapport från drivningen av TASS-tunneln. SKB R-10-31. Swedish Nuclear Fuel and Waste Management Co, Stockholm, Sweden

Konzuk JS, Kueper BH (2004) Evaluation of cubic law based models describing single-phase flow

through a rough-walled fracture. Water Resour Res 40 (2) doi:10.1029/2003wr002356
Lamas LN (1995) An Experimental Study of the Hydromechanical Properties of Granite Joints. Paper presented at the 8th ISRM Congress, September 25 - 29, 1995 Tokyo, Japan
Larsson E (1997) Groundwater flow through a natural fracture -flow experiments and numerical modelling. Licentiate thesis Chalmers University of Technology, Gothenburg, Sweden
Li B, Jiang Y, Koyama T, Jing L, Tanabashi Y (2008) Experimental study of the hydro-mechanical behavior of rock joints using a parallel-plate model containing contact areas and artificial fractures. Int J Rock Mech Min Sci 45 (3):362-375. doi:10.1016/j.ijrmms.2007.06.004
Makurat A, Barton N, Tunbridge L, Vik G (1990) The measurement of the mechanical and hydraulic properties of rock joints at different scales in the Stripa project. Paper presented at the International conference on rock joints, Loen, Norway
Munier R (1995) Studies of Geological Structures at Äspö: Comprehensive Summary of Results. Äspölaboratoriet Progress Report, vol 25-95-21. Swedish Nuclear Fuel and Waste Management Co, Stockholm, Sweden
Olsson M, Markström I, Pettersson A, Sträng M (2009) Examination of the Excavation Damaged Zone in the TASS tunnel, Äspö HRL. SKB R-09-39. Swedish Nuclear Fuel and Waste Management Co, Stockholm, Sweden
Olsson R, Barton N (2001) An improved model for hydromechanical coupling during shearing of rock joints. Int J Rock Mech Min Sci 38 (3):317-329. doi:10.1016/s1365-1609(00)00079-4
Pyrak-Nolte LJ, Myer LR, Cook NGW, Witherspoon PA (1987) Hydraulic and Mechanical Properties of Natural Fractures in Low Permeability Rock. Paper presented at the 6th ISRM Congress, August 30 - September 3, 1987, Montreal, Canada
Pyrak-Nolte LJ, Morris JP (2000) Single fractures under normal stress: The relation between fracture specific stiffness and fluid flow. Int J Rock Mech Min Sci 37 (1–2):245-262. doi:10.1016/S1365-1609(99)00104-5
Raven KG, Gale JE (1985) Water flow in a natural rock fracture as a function of stress and sample size. Int J Rock Mech Min Sci Geomech Abstr 22 (4):251-261. doi:10.1016/0148-9062(85)92952-3
Rhén I, Forsmark T, Hartley L, Jackson P, Roberts D, Swan D, Gylling B (2008) Hydrogeological conceptualisation and parameterisation, Site descriptive modelling SDM–Site Laxemar. SKB R-08-78. Swedish Nuclear Fuel and Waste Management Co, Stockholm, Sweden
Rhén I, Gustafson G, Stanfors R, Wikberg P (1997) Äspö HRL - Geoscientific evaluation 1997/5. Models based on site characterization 1986-1995. SKB TR 97-06. Swedish Nuclear Fuel and Waste Management Co, Stockholm, Sweden
Rocscience (2010) Examine 2D. 7 edn. www.rocscience.com, Toronto, Canada
Rutqvist J, Stephansson O (2003) The role of hydromechanical coupling in fractured rock engineering. Hydrogeol J 11 (1):7-40. doi:10.1007/s10040-002-0241-5
Snow DT (1968) Rock fracture spacings, openings and porosities. Proc Amer Soc Civil Engineers 94(SM1):73-79
Thörn J (2012) Coupling between changes in hydraulic and mechanical aperture: A laboratory study on rock cores. Report 2012:9. Chalmers University of Technology, Gothenburg, Sweden. Available at: http://cpl.lib.chalmers.se/publication/171899
Witherspoon PA, Wang JSY, Iwai K, Gale JE (1980) Validity of the cubic law for fluid flow in a deformable fracture. Water Resour Res 16 (6):1016-1024. doi:10.1029/WR016i006p01016
Zang A, Stephansson O (2010) Stress field of the Earth's crust. Springer, Dordrecht
Zimmerman R, Main I (2003) Chapter 7 Hydromechanical Behavior of Fractured Rocks. In: Yves G, Maurice B (eds) International Geophysics, vol Volume 89. Academic Press, pp 363-421
Zimmerman RW, Bodvarsson GS (1996) Hydraulic conductivity of rock fractures. Transport Porous Med 23 (1):1-30. doi:10.1007/bf00145263